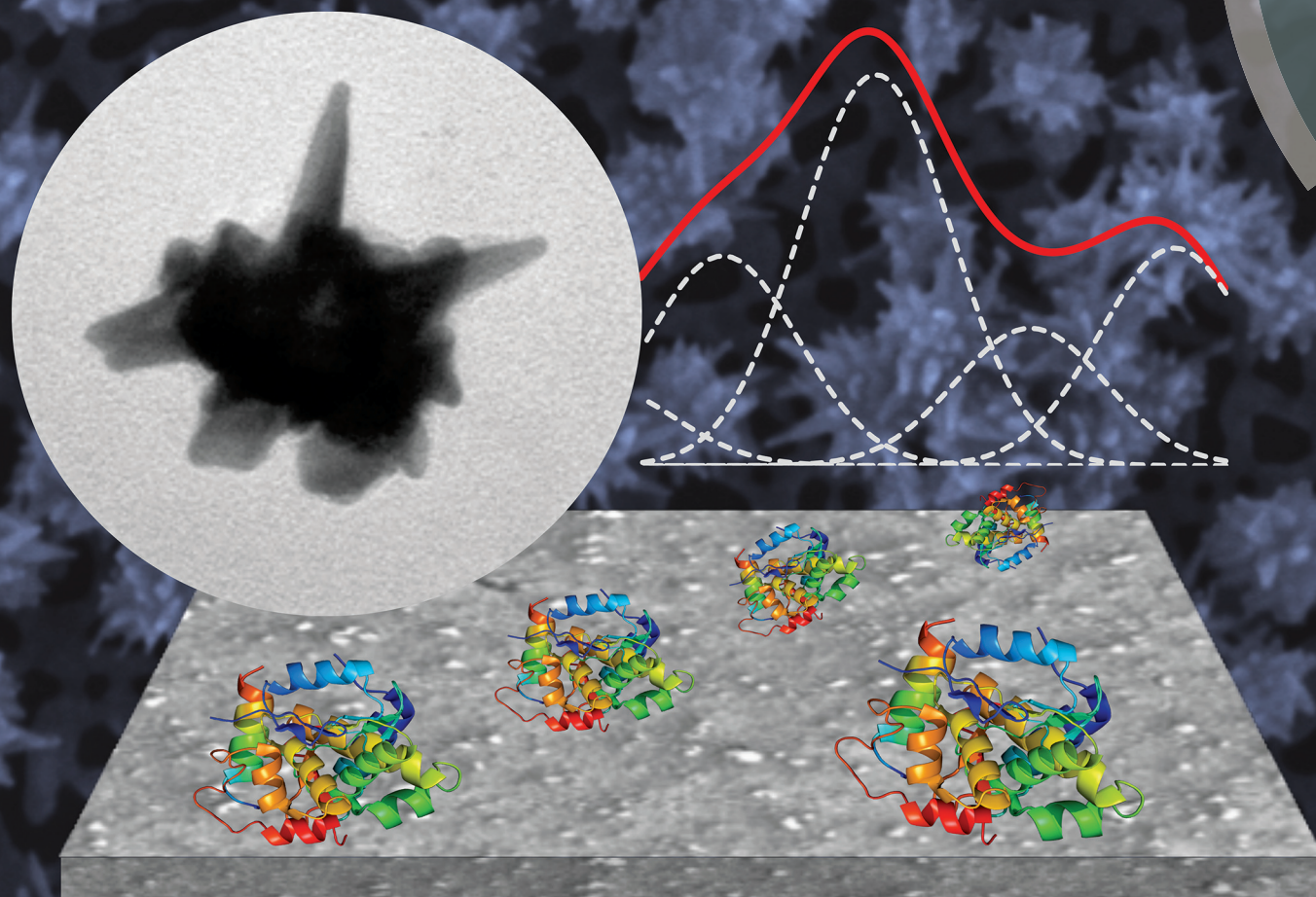


Analyst

rsc.li/analyst



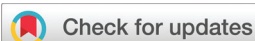
ISSN 0003-2654



PAPER

Ángela I. López-Lorente *et al.*

Gold-nanostar-based SERS substrates for studying protein aggregation processes



Cite this: *Analyst*, 2018, **143**, 5103

Gold-nanostar-based SERS substrates for studying protein aggregation processes†

Natalie Schwenk,^a Boris Mizaikoff,^a Soledad Cárdenas^b and Ángela I. López-Lorente^{b*}

Aggregation of proteins has been related to some neurodegenerative diseases such as Alzheimer's and Parkinson's among others. Raman spectroscopy is a useful technique for the investigation of protein conformation and of changes in their secondary structure. In this study, a surface enhanced Raman spectroscopy (SERS) substrate based on the immobilization of plasmonic gold nanostars on a glass slide *via* silanization of the surface has been prepared and characterized. Gold nanostars were synthesized *via* a seed-growth method using gold nanoparticles as seeds obtained *via* stainless steel as the reducing agent. The plasmonic substrate provided an enhancement of 5.7×10^2 fold, as shown for the Raman signal of crystal violet. Using this SERS-active substrate, the investigation of aggregation processes of bovine serum albumin (BSA) and myoglobin proteins upon temperature and solvent modification has been enabled with enhanced sensitivity. Both curve fitting and deconvolution of the amide I band, as well as 2D correlation analysis, were employed for the evaluation of the changes in the SERS spectra of the protein samples. The amide I band within the SERS spectra of the BSA protein revealed a decrease in the α -helix structures within the secondary structure of the protein while the presence of β -sheet structures increased with temperature and solvent concentration.

Received 30th April 2018,
Accepted 13th August 2018

DOI: 10.1039/c8an00804c

rsc.li/analyst

Introduction

Signal-enhancing vibrational spectroscopies including surface enhanced Raman spectroscopy (SERS) are of increasing interest in contemporary analytical spectroscopy. A variety of SERS-active substrates have been prepared from *e.g.* noble metal nanomaterials, including plasmon-resonant gold and silver nanoparticles (Au and Ag NPs, respectively). These substrates are based on nanoparticle aggregates, roughened surfaces as well as arrays of ordered nanoparticle schemes.¹ The increase in the electric field at the so-called “hot spots”,² consisting of two or more coupled metallic nanoparticles with closely spaced features,³ leads to an enhancement of the signal observed in Raman spectroscopy. Gold nanostars (AuNSts) are multi-branched nanoparticles, which can act as excellent amplifiers due to the presence of tips and sharp edges at their surface, thus creating a large number of hot spots. This nanomaterial has been recently introduced in enhanced vibrational

spectroscopies,⁴ *e.g.* for the detection of virus,⁵ molecular imaging⁶ and multiplex detection.⁷ Nevertheless, facile fabrication strategies for the preparation of reproducible SERS substrates with a large Raman enhancement are needed.

Aggregation of a variety of proteins has been associated with amyloid diseases including Alzheimer's, Parkinson's, and prion diseases (*e.g.* Creutzfeldt-Jakob). The aggregation of proteins has been investigated by a variety of techniques, including infrared (IR) spectroscopy,^{8–10} circular dichroism^{11,12} or fluorescence,^{13,14} among others. A limitation of conventional IR measurements is the achievable sensitivity resulting from the rather low intensity of conventional IR light sources, constricting the achievable signal-to-noise ratio, which has been overcome by developing new light sources *e.g.* quantum cascade lasers or the so-called “surface-enhanced infrared absorption spectroscopy” (SEIRAS).⁸ Raman spectroscopy and specially SERS due to the low Raman cross-section of proteins are useful spectroscopic techniques for the study of proteins since they can provide complementary information to previous techniques on the secondary structure of proteins, can be carried out over a wide spectral range and are insensitive to water, which is a limitation in IR since its features are in the same spectral range as the amide I band. The Raman spectrum of proteins is dominated by the so-called “amide I band” ($1600\text{--}1700\text{ cm}^{-1}$) arising primarily from the C=O vibration of amide bonds. The amide II band ($\sim 1550\text{ cm}^{-1}$) and the amide

^aInstitute of Analytical and Bioanalytical Chemistry, Ulm University, Ulm, Germany

^bDepartamento de Química Analítica, Instituto Universitario de Investigación en Química Fina y Nanoquímica IUIQFN, Universidad de Córdoba, Campus de Rabanales, Edificio Marie Curie Anexo, E-14071 Córdoba, Spain.

E-mail: q32loloa@uco.es

†Electronic supplementary information (ESI) available. See DOI: 10.1039/c8an00804c

III band consist of a combination of NH group bending vibrations and the C–N stretching vibration.¹⁵ In addition, amino acid residues such as phenylalanine, tryptophan, tyrosine and cysteine may also contribute to the Raman spectrum of proteins.

Two-dimensional (2D) correlation spectroscopy was introduced by Noda¹⁶ in 1990, adapting it from nuclear magnetic resonance and other resonance spectroscopy methods to vibrational spectroscopy. It is based on the detection of dynamic fluctuations in the spectral intensities induced by an external perturbation. Advantages of 2D IR are the simplification of complex spectra, improvement of spectral resolution and the gain of information from the deconvolution of information.¹⁶ 2D correlation spectroscopy in the infrared region has been used to study the effect of temperature on the structure of hemoglobin.¹⁷ Moreover, 2D Raman spectroscopy can also reveal useful information on protein structures.¹⁸

Herein, a straightforward procedure for the fabrication of a SERS-active substrate based on the immobilization of plasmonic gold nanostars on glass slides is presented. AuNSts were chemically grown from the seeds of AuNPs prepared mediated by stainless steel as the reducing agent,^{19,20} and subsequently immobilized at the glass surface *via* silanization. The SERS substrate has been characterized and the enhancement of the Raman signal has been evaluated using crystal violet as the model analyte. Furthermore, the substrate has been employed for the SERS study of the aggregation process of bovine serum albumin and myoglobin proteins induced by temperature and solvent. The presence of nanostars enables the adsorption of the protein owing to the affinity of thiol groups within the amino acid residues of the protein with the gold nanostars, and simultaneously provides enhanced sensitivity of the measurements as compared with bare glass. Evaluation of the spectra has been carried out both *via* Gaussian curve fitting of the amide I band of the proteins as well as *via* two dimensional correlation analysis in different spectral ranges, which have proven to provide complementary information, which is in agreement with the observed changes in solution, *i.e.* an increase in the content of crossed β -sheet structures.

Materials and methods

Reagents and materials

Lyophilized powder of myoglobin from equine heart and albumin from bovine serum (BSA) proteins were provided by Sigma-Aldrich Co. (Madrid, Spain) and used without further purification. 10 mg mL⁻¹ stock solutions of the proteins were prepared in Milli-Q Water (resistivity 18.2 M Ω cm at 25 °C; Millipore). Crystal violet was provided by Merck.

An AISI 304 (Fe/Cr18/Ni10) stainless steel disc (diameter 8 mm, thickness of 0.5 mm) provided by GoodFellow (Cambridge, United Kingdom) was employed as a solid reducing agent for the formation of gold nanoparticles.

The chemicals used for the synthesis of the nanomaterials and substrate functionalization were all also obtained from

Sigma-Aldrich Co., namely 3-aminopropyltriethoxysilane (APTES), gold(III) chloride trihydrate, silver nitrate, ascorbic acid (AA) and all common solvents.

Synthesis of bare gold nanoparticles mediated by stainless steel

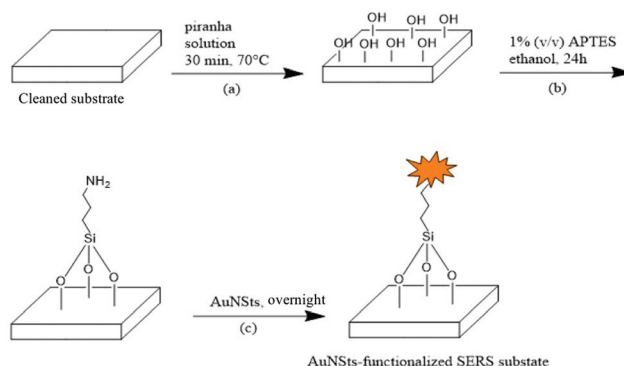
Gold nanoparticles were prepared using stainless steel as the solid reducing agent following a similar procedure to that described in ref. 19 and 20 with some modifications. The spherical gold nanoparticles were synthesized by vigorous stirring for 8 minutes of 200 μ L gold(III) chloride trihydrate (0.1%) in contact with an AISI 304 (Fe/Cr18/Ni10) stainless steel disc (diameter 8 mm, thickness of 0.5 mm). The use of steel leads to the formation of AuNPs without any ligand on their surface.

Formation of the gold nanostars

Star-shaped gold nanoparticles (AuNSts) were synthesized using a seed-mediated method by chemical reduction of Au(III) similar to that reported by O. Bibikova *et al.*^{4,21} Briefly, 0.25 mL of 30 mM HAuCl₄ (1%) and 9.75 mL MilliQ Water were stirred at room temperature. Then 30 μ L 1 M HCl and 300 μ L of the freshly prepared spherical gold nanoparticles were added. After that 300 μ L of 2 mM AgNO₃ and 150 μ L of 0.1 M AA were added simultaneously and further stirred for a few seconds. A color change from slightly red to dark gray was observed.

AuNSt functionalization on the glass substrate

The gold nanostars were functionalized on the glass substrate following a protocol by Kyaw *et al.*²² The functionalization process is shown in Scheme 1. First, the glass substrates were cleaned by sonication in soap water, ethanol, acetone and deionized water for 20 minutes each and dried in an oven at \sim 80 °C. The clean and dry substrates were immersed in freshly prepared piranha solution (30% H₂O₂ and 96% H₂SO₄, 1 : 3) at \sim 70 °C for 30 minutes. Afterwards the glass substrates were rinsed with deionized water and dried again at \sim 80 °C. Then



Scheme 1 Scheme of the functionalization process of the glass substrate with AuNSts, which comprises (a) activation of the glass with piranha solution, (b) 24 h incubation in 1% (v/v) APTES and (c) overnight incubation in the AuNSt solution. For further details about the cleaning procedures between the different steps, see the text.

they were immersed in 1% (v/v) solution of 3-aminopropyltriethoxysilane (APTES) in absolute ethanol for ~24 h at room temperature. In order to remove any physisorbed APTES molecules the functionalized glass substrates were then sonicated with ethanol and deionized water for 5 minutes each and dried at ~80 °C. For the deposition of the AuNSts, the substrates were immersed in 3 mL of the AuNSts solution overnight. Then the AuNSts-functionalized SERS substrate was rinsed with deionized water and carefully dried under a N₂ gas stream.

Characterization of the SERS substrates

UV/Vis measurements of the gold nanoparticles were performed using a halogen lamp as the light source, and a monochromator combined with a photonic detector of a PTI Fluorescence Master System as the detector.

The concentrations of gold nanoparticles and gold nanostars were calculated *via* inductively coupled plasma-mass spectrometry (ICP-MS) (PerkinElmer NexionX), carried out at the Central Support Service for Research of University of Córdoba (SCAI, UCO).

Microscopic characterization was performed both *via* transmission electron microscopy (TEM) by using a JEOL JEM 1400 microscope and scanning electron microscopy (SEM) with a JEOL JSM 6300 microscope (SCAI, UCO). A drop of the synthesized gold nanoparticle suspension was drop-cast on a carbon TEM grid with a Carbowax forward. The particle size distribution was analyzed by measuring 1659 nanoparticles from the TEM micrographs using ImageJ Software.

Surface enhanced Raman spectroscopy

Raman and SERS measurements were performed by using a confocal Raman spectrometer (alpha500, Witec GmbH, Ulm, Germany). With the combination of a highly efficient Raman spectrometer and a high resolution confocal optical microscope it is not only possible to obtain a Raman spectrum from a particular sample, but to combine this chemical information with spatial resolution in the sub-micrometer regime.

The sample was excited with a frequency doubled Nd:YAG laser at 532 nm (second harmonic generation) at a laser power of 13.5 mW (measured prior to the objective lens). The laser beam was focused on the sample using a 20×/0.4 Zeiss objective. Raman spectra were collected using a 600 g mm⁻¹ diffraction grating and an electron-multiplying (EM) CCD camera. Spectra were acquired with an integration time of 1 s, averaging a total of 10 spectra. 2 μL of the protein solution were drop-cast onto the 50 °C heated nanostar-modified SERS substrate so that evaporation of the solvent occurs rapidly.

The samples of BSA and myoglobin proteins (10 mg mL⁻¹) were always deposited on the SERS substrate using the same procedure. 2 μL of the sample was dropped onto the AuNSt-functionalized SERS substrate and immediately heated at about 50 °C to ensure homogeneous evaporation. Spectra were acquired at different locations within the center of the spot, in order to avoid the possible effects of the drying pattern, and the average value was calculated.

Aggregation of protein samples

Aggregation of the proteins was induced by a temperature increase⁹ as well as by different concentrations of dimethylsulfoxide (DMSO). For the temperature induced aggregation 50 μL of eight aqueous solutions of each protein were incubated in a water bath for 2 hours in the range 20–90 °C with a 10-degree increase followed by room-temperature recovery. The solvent-induced aggregation was reached by dissolving the protein in an aqueous solution containing different concentrations, *i.e.* 1, 2, 3, 4 and 5% of DMSO.

Data analysis

Raman spectra were analyzed with PeakFit software (Systat Software Inc., San Jose, CA). First of all, baseline correction was performed followed by smoothing with 20% Fast Fourier Transform (FFT) filtering. The region 1600–1700 cm⁻¹ of BSA protein spectra in different temperature treatments were analyzed using second derivative and Gaussian peak fitting, followed by deconvolution into sub-peaks performed *via* PeakFit software.

Two-dimensional (2D) correlation spectroscopy is based on the detection of dynamic fluctuations in the spectral intensities induced by an external perturbation. After inducing a series of perturbations on the system (*i.e.* temperature variation, solvent modification), spectra are collected in a sequential order and subsequently analysed *via* 2D correlation as follows. First of all, spectra were subjected to baseline correction, smoothing and normalization in the range 1600–1720 cm⁻¹ and 600–1060 for BSA and 1500–1700 cm⁻¹ for myoglobin protein, *via* MATLAB Toolbox. 2D correlation maps were created using 2DShige software and MATLAB. Synchronous correlation intensities were computed for the IR spectra at different temperatures by applying the generalized 2D correlation algorithm of Noda.¹⁶ For the 2D analysis spectra, the external perturbations considered were the temperature of incubation and solvent composition. In the synchronous map, autopeaks appear at the diagonal positions and reflect the changes in intensity in the spectra for these regions upon external perturbation.²³ Fig. 1 schematically illustrates the protein spectra data-treatment routines.

Results and discussion

Characterization of the gold nanoparticles

AuNPs synthesized using stainless steel as a solid reducing agent were characterized *via* transmission electron microscopy (TEM) in order to determine their size and shape. As can be seen in Fig. 2a, AuNPs are well dispersed in solution with a polygonal yet nearly spherical shape. The average size of the nanoparticles was calculated using ImageJ software for the analysis of the AuNPs in the TEM images measuring a total of 1658 NPs, resulting in a diameter of 37 ± 17 nm. The concentration of gold in the AuNP solution as determined by inductively coupled plasma-mass spectrometry (ICP-MS) after acid digestion of the sample with HNO₃ 69% and HCl 37% 3 : 1 was 84 mg L⁻¹. In addition, Z-potential measurements of AuNPs

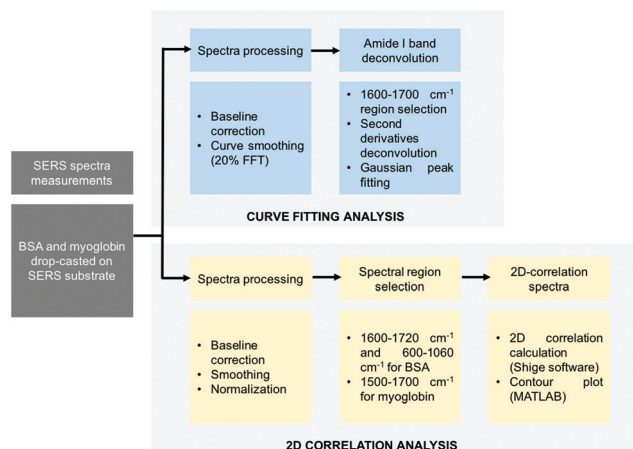


Fig. 1 Scheme of the data treatment routines for both curve fitting and 2D correlation analyses of the SERS spectra of BSA and myoglobin proteins.

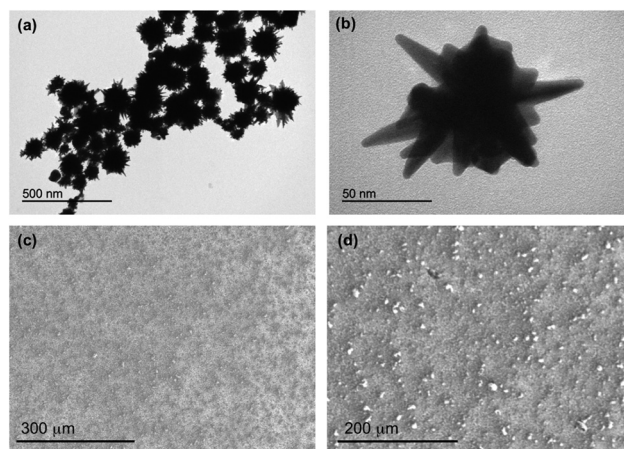


Fig. 3 (a) and (b) TEM images of the synthesized AuNSts. (c) and (d) SEM images of the AuNSts deposited at the APTES-modified glass forming the SERS active substrate.

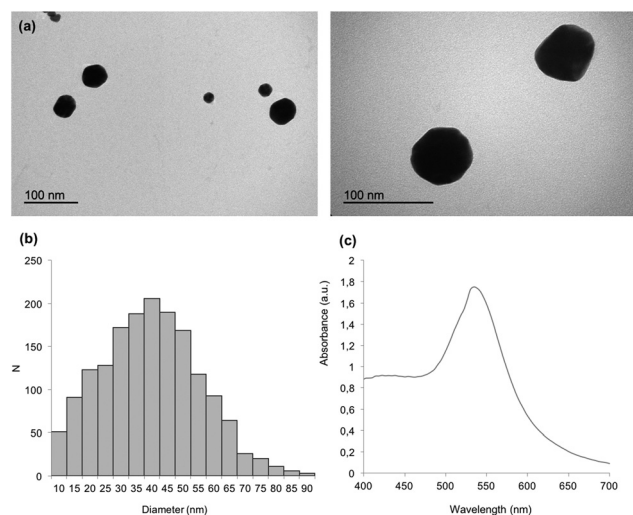


Fig. 2 (a) TEM images of collected individual bare gold nanoparticles obtained mediated by stainless steel. (b) Histogram of the size distribution of the AuNPs. (c) UV-vis spectrum of the AuNPs in aqueous solution showing the plasmon resonance band at around 534 nm.

revealed that such NPs are positively charged with a potential of 26.9 mV.

Gold nanoparticles were also characterized *via* UV-vis spectroscopy (Fig. 2c) showing the characteristic plasmon resonance band of the AuNPs with a maximum at 534 nm, which is in agreement with the average size calculated from the TEM images.

Characterization of the gold nanostars and SERS substrate

As previously described, gold nanostars were prepared *via* a seed-mediated method using bare gold nanoparticles synthesized using stainless steel as the solid reducing agent. The morphology of the synthesized AuNSts was evaluated *via* TEM microscopy. Fig. 3a and b show the micrographs of the

obtained nanostars, which have an outer diameter of approximately 53 nm revealing several spikes with an average size of 20 nm emanating from their surface. The concentration of gold in the AuNSt solution determined *via* ICP-MS analogous to that previously described for the AuNPs was 135 mg L^{-1} .

The SERS substrate composed of gold nanostars immobilized on a glass slide was further investigated *via* SEM microscopy, showing aggregates of nanostars deposited on the glass surface. The functionalization of the slides with the nanostars was carried out following the procedure described in detail above. Briefly, after cleaning the glass with soap water, ethanol, acetone and deionized water and drying it, the glass slide was subjected to a pre-treatment in piranha solution in order to activate the hydroxyl groups at its surface, thus enabling the subsequent attachment of a 3-aminopropyltriethoxysilane layer which provides the binding sites for the AuNSts owing to the affinity of gold towards the amino groups.^{22,24} The main advantage of the chemical deposition of the AuNSts onto the glass surface is their adhesion to the substrate, improving the stability of the SERS substrate. The AuNSt-functionalized SERS substrates were rinsed with deionized water, observing that the AuNSts are attached to the surface and there are no losses during the incubation of the analyte or the cleaning process.

SERS enhancement *via* gold-nanostar-modified substrates

The enhancement produced by the presence of the plasmonic gold nanostars with their antennas deposited at the SERS substrate was first evaluated using crystal violet (CV) as the model analyte. CV is a dye which is usually employed in SERS studies due to its reduced fluorescence. The bands observed in the SERS and Raman spectra in Fig. 4 can be ascribed to the stretching vibration of nitrogen and the phenyl ring (1374.9 cm^{-1}), and the in-plane aromatic C-C vibrations, originating two bands at about 1600 cm^{-1} . Moreover, in the low region of the spectrum bands at around 416 cm^{-1} , 517 cm^{-1} ,

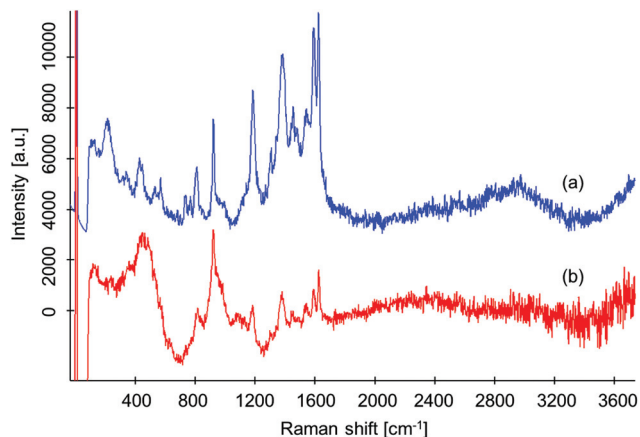


Fig. 4 Comparison of the SERS spectra of 25 mg L⁻¹ CV on top of the SERS substrate (a) with the Raman spectra of 1000 mg L⁻¹ CV on the bare glass substrate (b).

554 cm⁻¹, 720 cm⁻¹ appear, which can be assigned to the out-of-plane bending of the C-C_{center}-C, the bending mode of the C-N-C bonds, the out-of-plane aromatic C-C deformation and the C-N-C symmetric stretching, respectively. The bands related to the C-H bending modes can be observed at 910 and 1181 cm⁻¹, corresponding to the out-of-plane and in-plane modes, respectively, the latter one being used in order to calculate the enhancement of the Raman signal produced by the substrate.

The enhancement factor for the Raman signal of CV *via* the gold-nanostar-based SERS substrate was calculated by comparing the intensities of the Raman spectra of CV deposited on the bare glass and on the SERS substrate. The concentration of CV solution detectable on glass was 1000 mg L⁻¹, while within the SERS substrate lower concentrations (*e.g.* 25 mg L⁻¹) can be measured. Fig. 4a shows the SERS spectra of CV after the deposition of 2 μL of a 25 mg L⁻¹ CV solution on the SERS active substrate as well as the Raman spectrum of 2 μL of a 1000 mg L⁻¹ CV solution on the bare glass slide. Both spectra were compared and the enhancement factor (EF) was calculated according to the following equation:²⁵

$$EF = (I_{\text{SERS}}/I_{\text{Raman}}) \times (N_{\text{Raman}}/N_{\text{SERS}}),$$

where *I* is the intensity (*i.e.* the peak height of the selected band, and in this case, the band at 1181 cm⁻¹ due to the C-H bending was selected) whereas *N* represents the total number of analyte molecules deposited on the AuNSt modified SERS substrate and bare glass, which has been directly related to the concentration of CV deposited in each case. According to the above equation, an enhancement factor of 5.7×10^2 was obtained with the plasmonic AuNSt SERS substrate compared to the bare glass slide.

Moreover, the enhancement factor observed for proteins was also calculated for BSA similarly to that for CV, obtaining a 20-fold EF of the Raman signal of BSA protein. Fig. S1 (ESI[†]) shows the Raman and SERS spectra of BSA protein on glass and the SERS substrate, respectively. It should be pointed out

that in the case of the Raman spectra, even at a concentration of 25 mg mL⁻¹, the signal was relatively low and with a high signal-to-noise ratio, while the presence of the gold nanostars enabled the acquisition of SERS spectra with an acceptable signal-to-noise ratio in order to perform the subsequent curve fitting and 2D analysis of the spectra. Thus, although the concentration of protein could have been reduced in the SERS measurements, a concentration of 10 mg mL⁻¹ was selected in order to have spectra with a good signal-to-noise ratio for further analysis.

SERS spectra of myoglobin and bovine serum albumin

Bovine serum albumin (BSA) is a globular protein composed of 583 amino acids. Its secondary structure is mainly dominated by alpha helix structures, which accounts for approximately 67% of its structure. BSA protein was selected owing to its affinity towards gold nanoparticles, since it possesses an external thiol group at position 34 from the cysteine residue available for conjugation to the gold surface and has 17 disulfide bridges.²⁶ As is evident in Fig. 5a, the SERS spectrum

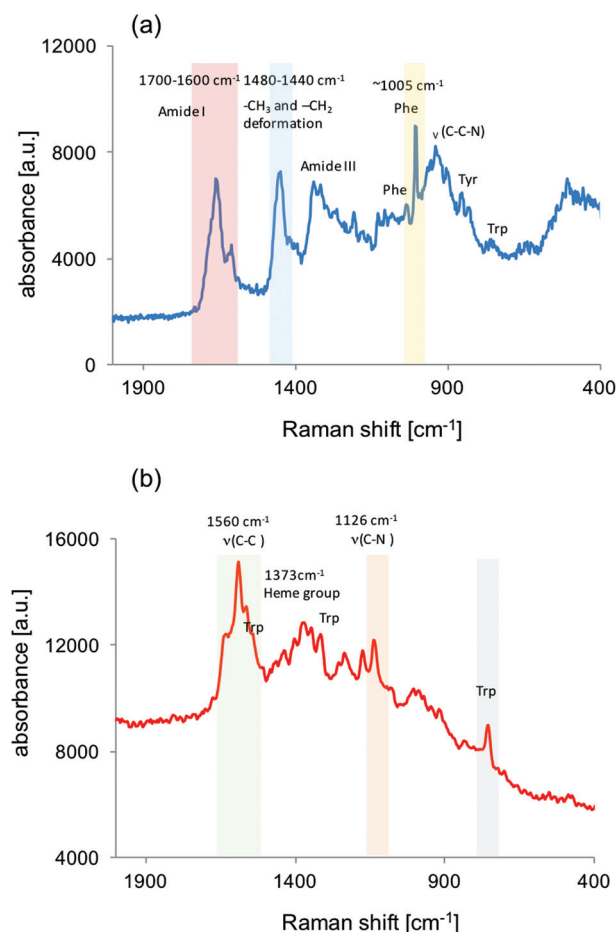


Fig. 5 (a) SERS spectrum of BSA after deposition of 2 μL of a 10 mg mL⁻¹ BSA solution on the SERS substrate composed of gold nanostars. (b) SERS spectrum of myoglobin after deposition of 2 μL of a 10 mg mL⁻¹ MG solution on the SERS substrate. SERS conditions: 1 s integration time with 10 acquisitions, laser power 13.5 mW.

of BSA is dominated by the band arising from the amide bonds ($\nu\text{C=O}$ vibration), the so-called “amide I band” at about $1600\text{--}1700\text{ cm}^{-1}$.

Moreover, in the region of $1440\text{--}1480\text{ cm}^{-1}$, bands corresponding to the $-\text{CH}_3$ and $-\text{CH}_2$ deformation from the amino acid side chains are observed, whereas the symmetric stretching of the carboxylic group is reported to originate a band around 1420 cm^{-1} . The so-called “amide III band” was reported at around $1230\text{--}1300\text{ cm}^{-1}$, arising from both the in-plane NH group bending vibration and the C–N stretching vibration.²⁷ In addition, the different amino acids also contribute to the SERS spectra, such as phenylalanine (Phe), tryptophan (Trp), tyrosine (Tyr) and cysteine (Cys). As can be observed in the spectra shown in Fig. 5a, the major contribution of amino acids is the band at about 1005 cm^{-1} , together with that at about 1033 cm^{-1} arising from Phe. Moreover, the bands at about 855 and 830 cm^{-1} originated from Tyr, while the band at $\sim 754\text{ cm}^{-1}$ arose from Trp. The small shoulder observed at about 645 cm^{-1} is associated with Tyr residues. In this region there is also a band at about 930 cm^{-1} , which arises from the $\nu(\text{C-C-N})_{\text{sym}}$, skeletal vibrations associated with α -helix structures.^{28,29}

On the other hand, myoglobin is a protein whose secondary structure is $\sim 75\%$ alpha-helix structures consisting of 153 amino acids. Myoglobin lacks cysteine residues, which makes the formation of covalent bonds with the AuNst surface through thiol interaction impossible, the interaction being led by electrostatic and hydrophobic interactions.³⁰ It contains a Fe-protoporphyrin prosthetic heme group within the polypeptide chains. As depicted in Fig. 5b, the SERS spectrum of myoglobin is dominated by a band at about 1560 cm^{-1} , which has been attributed to the C–C vibrational band.³¹ In addition, the band at about 1126 cm^{-1} can be observed arising from the C–N stretching, whereas that at around 1373 cm^{-1} is an oxidation marker of the heme group. On the other hand, bands arising from the aromatic amino acid residues such as those at 760 cm^{-1} , 1365 cm^{-1} together with a shoulder at $\sim 1555\text{ cm}^{-1}$ correspond to Trp residues.

SERS study of protein aggregation induced by temperature

Amyloid aggregation of proteins has been related to amyloid or prion diseases, such as neurodegenerative diseases *e.g.* Alzheimer's, Parkinson's or Creutzfeldt–Jakob disease. Different factors such as temperature increase or solvents may induce the aggregation of proteins, which is reflected by an increase of crossed β -sheet structures within the secondary structure of the protein.

The amide I band of proteins is sensitive to the changes in the secondary structure of the protein, such as aggregation processes and the formation of fibrils. As previously mentioned, the BSA secondary structure is dominated by $\sim 67\%$ of alpha-helix structures, while containing approximately 18% of beta sheet as well as random coil structures. As can be seen in Fig. 6a, changes in temperature until about $70\text{--}80\text{ }^\circ\text{C}$ did not dramatically change the amide I band of the BSA protein. According to the literature, the modification of the secondary

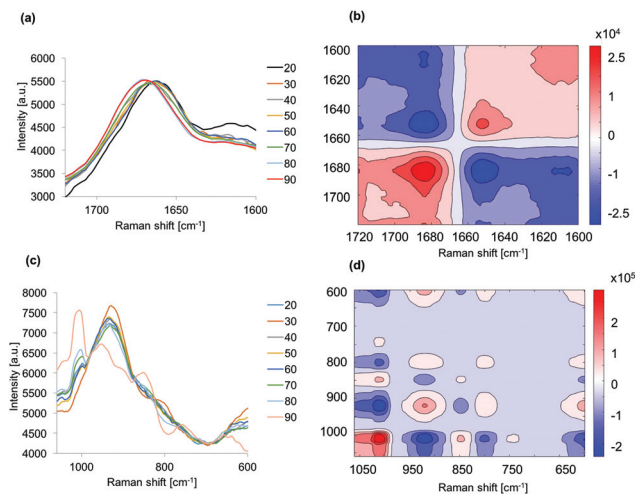


Fig. 6 (a) SERS spectra in the region $1600\text{--}1720\text{ cm}^{-1}$ of BSA protein after incubation at different temperatures ($^\circ\text{C}$). Spectra were subjected to smoothing and normalization. (b) Synchronous 2D-correlation spectrum in the range $1600\text{--}1720\text{ cm}^{-1}$ with temperature as the external perturbation. (c) SERS spectra in the region $600\text{--}1060\text{ cm}^{-1}$ of BSA protein after incubation at different temperatures ($^\circ\text{C}$). Spectra were subjected to smoothing and normalization. (d) Corresponding synchronous 2D-correlation spectrum in the range $600\text{--}1060\text{ cm}^{-1}$ with temperature as the external perturbation.

structure of BSA starts at about $60\text{ }^\circ\text{C}$.¹⁸ As reported in the literature, the band at around 1630 cm^{-1} within the amide I band of the BSA Raman spectrum is related to intermolecular β -sheet structures, while the band at about 1675 cm^{-1} has been related to the intra-molecular β -sheet within the protein.¹⁸ On the other hand, the band at around 1653 cm^{-1} in this region has been associated with α -helical peptide bonds.³² As shown in Fig. 6a, the increase in temperature leads to changes in the amide I region of the SERS spectra, the peak maximum being shifted from $\sim 1653\text{ cm}^{-1}$ to 1675 cm^{-1} , which is in agreement with the formation of β -sheet structures upon aggregation of the protein. A higher frequency mode at $\sim 1675\text{ cm}^{-1}$ can be identified as the in phase $\nu(\text{C=O})$ of the carbonyls in the β -sheets.³²

The change in the secondary structure of BSA protein upon heating was also evaluated *via* 2D correlation of the SERS spectra focusing on the amide I region $1600\text{--}1700\text{ cm}^{-1}$ related to the secondary structure of the protein, as discussed. Two-dimensional correlation spectroscopy is a useful technique for the detection of dynamic fluctuations in the spectra induced by an external perturbation. Fig. 6b shows the synchronous correlation spectra of BSA protein SERS spectra in the amide I band region with temperature as external perturbation. 2D correlation autopeaks (red) appear at around ~ 1653 and $\sim 1680\text{ cm}^{-1}$, indicating that changes within the secondary structure of BSA take place upon increasing the temperature. The presence of two negative (blue) crosspeaks indicates that the intensity changes of the two autopeaks occur in opposite directions, *i.e.* while one of the bands is increasing (1680 cm^{-1}) the other one is decreasing in intensity (1653 cm^{-1}).

In addition to the amide I region of the protein spectrum, the region compressed between 600 and 1060 cm^{-1} was also evaluated. As depicted in Fig. 6c, upon heating, changes in this region are observed, *i.e.* mainly in the band at 1004 cm^{-1} of Phe, at ~ 855 and 645 cm^{-1} due to Tyr residues and at ~ 759 cm^{-1} arising from Trp. Furthermore, as can be observed in the figure, the band at about 930 cm^{-1} , related to the $\nu(\text{C}-\text{N})_{\text{sym}}$ skeletal vibrations associated with the α -helix structures, is significantly reduced when the temperature reaches 90 $^{\circ}\text{C}$, which is in accordance with the decrease in the α -helix content also observed in the amide I band region. The 2D correlation spectrum was also calculated (Fig. 6d), showing autopeaks in the region at ~ 1005 cm^{-1} and 930 cm^{-1} along with the region ~ 850 and 800 cm^{-1} albeit with less intensity. The negative (blue) crosspeaks in the regions (1005, 930 cm^{-1}) and (930, 1005 cm^{-1}) indicate that both bands vary in opposite directions.

Moreover, curve fitting and deconvolution of the amide I band region (1600–1700 cm^{-1}) of the BSA SERS spectra were also performed, as depicted in Fig. 7. The amide I band of the

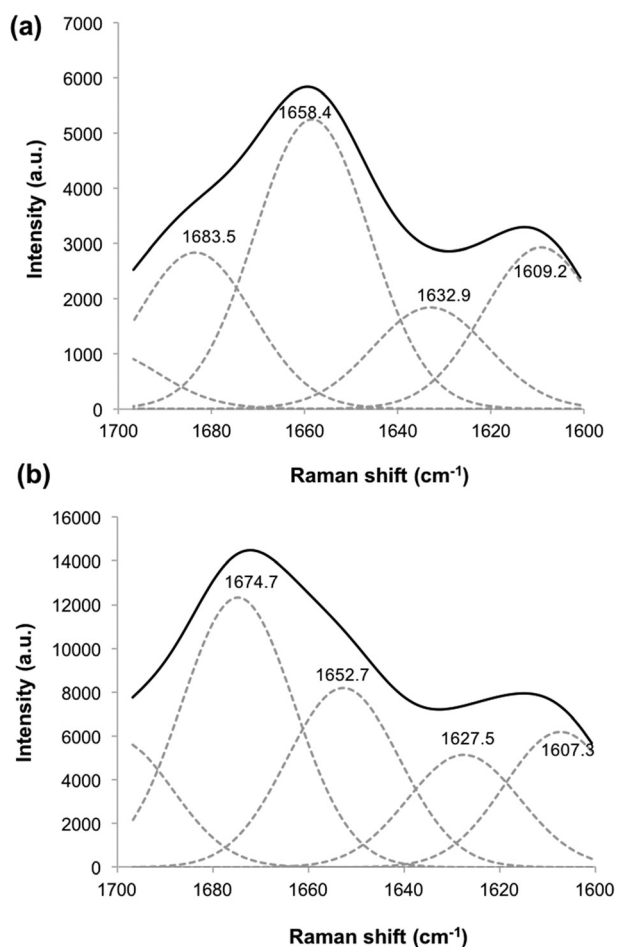


Fig. 7 Curve fitting of the band at 1600–1700 cm^{-1} in the SERS spectrum of BSA protein deposited on the SERS substrate (a) globular protein at room temperature and (b) after incubation for 2 h in a water bath at 90 $^{\circ}\text{C}$.

native globular BSA protein (Fig. 7a) shows the main contribution from the peak at about 1658 cm^{-1} , related to the α -helix structures. Sub-peaks at about 1683, 1632 and 1609 cm^{-1} are also deconvoluted (curve fitting with $r^2 = 0.999$). The bands in the region 1604–1615 cm^{-1} are associated with the ring modes from aromatic residues, *i.e.* Phe and Tyr, while that at ~ 1630 cm^{-1} , as previously stated, is related to intermolecular β -sheet structures. On the other hand, the curve fitting and deconvolution of the amide I band of BSA protein after incubation at 90 $^{\circ}\text{C}$ (Fig. 7b) revealed the presence of sub-peaks at about 1607, 1627, 1653 and 1675 cm^{-1} (curve fitting with $r^2 = 0.998$), the latter contributing to a major extent to the entire band. The sharp decrease in the sub-peak around 1653 cm^{-1} and the subsequent increase of the sub-peak at about 1675 cm^{-1} as compared with the protein at room temperature are consequences of the formation of the aggregates and the decrease in the α -helix structure content along with the increase in β -sheet features within the aggregates. Herein it has been assumed that the Raman cross-sections of each secondary conformation contribute identically to the spectra, and thus the integrated band intensities of the amide I band can be correlated with the fraction of each secondary structure.^{32,33}

In addition, myoglobin protein solutions were also incubated in a water bath at different temperatures and the subsequent SERS spectra were recorded. Fig. 8a depicts the SERS spectra of myoglobin after different temperature treatments in the region 1500–1700 cm^{-1} . As previously described, it has been reported that in this region the C–C vibrational bands at about 1560 cm^{-1} are observed, together with contributions of Trp residues at values about 1555 cm^{-1} (ref. 18) (laser wavelength 830 nm, note that herein the laser wavelength used is 532 nm). The tryptophan residues in myoglobin protein are reported to be located in an α -helix separated from the heme by the E helix.³⁴ Moreover, the contributions of parallel/anti-parallel β -sheet structures at ~ 1550 cm^{-1} are also reported to contribute to the amide II band of proteins.³⁵ As can be observed in Fig. 8a, with an increase in temperature both a shift from a maximum at about 1586 cm^{-1} to 1581 cm^{-1} as well as an increase in the region 1520–1540 cm^{-1} occur, as reflected by an autopeak in the synchronous 2D correlation spectrum (Fig. 8b). In addition, a decrease in the maximum around 1585–1580 cm^{-1} and at about 1640 cm^{-1} occurs, which correspond to the two other autopeaks in spectrum of Fig. 8b. The negative (blue) crosspeaks in the spectrum confirm that the intensity in the low region of the spectrum is increasing while that of ~ 1600 cm^{-1} and ~ 1640 cm^{-1} is decreasing. On the other hand, the positive (red) crosspeaks for the pairs (1600, 1640 cm^{-1}) and *vice versa* show that both bands show the same tendency of evolution with the external perturbation, *i.e.* temperature.

Solvent induced aggregation of proteins

Solvent conditions play an important role in the physical properties of proteins in solution. Previous studies have been carried out in aqueous solution, since water is the most con-

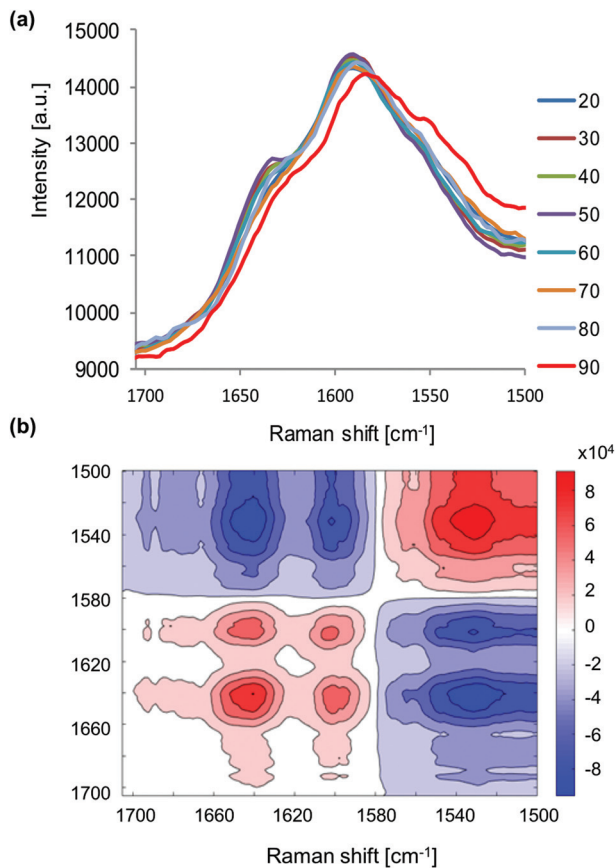


Fig. 8 (a) SERS spectra in the region 1500–1700 cm^{-1} of myoglobin protein after incubation at different temperatures ($^{\circ}\text{C}$). Spectra were subjected to smoothing and normalization. (b) Corresponding synchronous 2D-correlation spectrum with temperature as the external perturbation.

venient solvent in terms of spectral contributions, as it is a weak Raman scatterer, leading to little or no interference from water in the Raman spectra. Organic solvents, dimethyl sulfoxide (DMSO) among them, have been used to induce precipitation, aggregation³⁶ and denaturalization of proteins, and structural changes and unfolding of the proteins were observed when increasing the DMSO concentration.^{37,38}

Solvent-induced aggregation of proteins was, thus, next investigated by using DMSO at different concentrations in the range 1–5% in aqueous solution. As can be observed in Fig. 9a, the tendency with increasing concentration of solvent is similar to that of temperature, *i.e.* a shift in the peak maximum from $\sim 1668 \text{ cm}^{-1}$ to 1673 cm^{-1} , as a consequence of the formation of β -sheet structures upon aggregation of the protein. It has to be pointed out that 1% of DMSO already led to an increase in β -sheet structures as compared with untreated protein showing the maximum at about 1653 cm^{-1} (see Fig. S5, ESI[†]). The 2D correlation spectrum in Fig. 9b shows autopeaks at $\sim 1655 \text{ cm}^{-1}$ and within the region $1675\text{--}1700 \text{ cm}^{-1}$, which is also in agreement with that previously discussed for increasing temperature. Also the observed changes in the low region ~ 1604 and 1615 cm^{-1} are

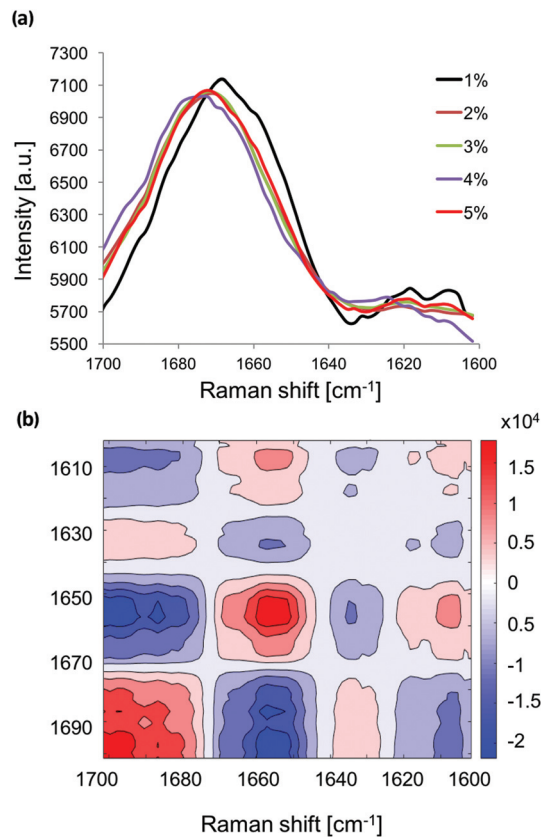


Fig. 9 (a) Raman spectra in the region 1700–1600 cm^{-1} of BSA protein after treatment with different amounts of DMSO (1–5%). Spectra were subjected to smoothing and normalization in the PLS toolbox. (b) Corresponding synchronous 2D-correlation spectrum.

related to the ring modes of aromatic residues, which may change due to the different solvent environments. In the case of solvent induced aggregation of myoglobin protein, similar behaviour to that described by temperature induced aggregation is observed. Further details can be found in the ESI.[†]

Conclusions

A plasmonic SERS active substrate based on the immobilization of gold nanostars prepared *via* a seed-mediated synthesis using bare gold nanoparticles obtained with stainless steel as the reducing agent has been developed and applied to studies of the aggregation behaviour of proteins. The thus prepared SERS substrate provided useful enhancement factors of approximately 5.7×10^2 as compared with bare glass using crystal violet as the model analyte. Moreover, the substrate enabled the acquisition of the SERS spectra of bovine serum albumin and myoglobin proteins.

Aggregation of both proteins was induced *via* temperature increase and solvent modification, *i.e.*, by the addition of various concentrations of dimethylsulfoxide. The changes within the secondary structure of the proteins upon aggregation were evaluated *via* curve fitting of the amide I band of the

protein, which is related to its secondary structure, as well as by analysing the synchronous 2D correlation SERS spectrum within the region of interest. The increase in temperature led to changes in the amide I region of the SERS spectra of BSA, the peak maximum being shifted from $\sim 1653\text{ cm}^{-1}$ to 1675 cm^{-1} , which is in agreement with the formation of β -sheet structures upon aggregation of the protein, which was confirmed by the increase in the sub-peak at about 1675 cm^{-1} within the deconvoluted spectra at $90\text{ }^\circ\text{C}$. Similar results were found *via* solvent-induced aggregation, which is also reflected in an increase in the spectral features related to β -sheet structures.

Conflicts of interest

There are no conflicts to declare.

Acknowledgements

A. I. López-Lorente acknowledges the Ministry of Education of Spain for a *Juan de la Cierva* contract (IJCI-2015-23994) at the University of Córdoba (Spain). A. I. López-Lorente and S. Cárdenas wish to thank Spain's Ministry of Education, Culture and Sport for funding the project (CTQ2017-83175-R).

References

- H. Ko, S. Singamaneni and V. Tsukruk, *Small*, 2008, **4**, 1576–1599.
- J. Haes, S. Zou, G. C. Schatz and R. P. Van Duyne, *J. Phys. Chem. B*, 2004, **108**, 6961–6968.
- X. Lang, T. Qiu, W. Zhang, C. Ji, J. Wang and P. K. Chu, *J. Phys. D: Appl. Phys.*, 2010, **43**, 455302.
- O. Bibikova, J. Haas, A. I. López-Lorente, A. Popov, M. Kinnunen, Y. Ryabchikov, A. Kabashin, I. Meglinski and B. Mizaikoff, *Anal. Chim. Acta*, 2017, **990**, 141–149.
- M. Reyes, M. Piotrowski, S. K. Ang, J. Chan, S. He, J. J. H. Chu and J. C. Y. Kah, *Anal. Chem.*, 2017, **89**, 5373–5381.
- Y. Liu, H. Yuan, A. M. Fales, J. K. Register and T. Vo-Dinh, *Front. Chem.*, 2015, **3**, 51.
- H. Yuan, Y. Liu, A. M. Fales, Y. L. Li, J. Liu and T. Vo-Dinh, *Anal. Chem.*, 2013, **85**, 208–212.
- A. I. López-Lorente and B. Mizaikoff, *Anal. Bioanal. Chem.*, 2016, **408**, 2875–2889.
- P. Wang, W. Bohr, M. Otto, K. M. Danzer and B. Mizaikoff, *Anal. Bioanal. Chem.*, 2015, **407**, 4015–4021.
- A. I. López-Lorente, P. Wang, M. Sieger, E. Vargas Catalan, M. Karlsson, F. Nikolajeff, L. Österlund and B. Mizaikoff, *Phys. Status Solidi A*, 2016, **213**, 2117–2123.
- S. Benjwal, S. Verma, K. H. Röhm and O. Gursky, *Protein Sci.*, 2006, **15**, 635–639.
- V. Joshi, T. Shivach, N. Yadav and A. S. Rathore, *Anal. Chem.*, 2014, **86**, 11606–11613.
- F. Hillger, D. Nettels, S. Dorsch and B. Schuler, *J. Fluoresc.*, 2007, **17**, 759–765.
- C. A. Royer, *Chem. Rev.*, 2006, **106**, 1769–1784.
- D. Kurouski, R. P. Van Duyne and I. K. Lednev, *Analyst*, 2015, **140**, 4967–4980.
- I. Noda, *Appl. Spectrosc.*, 1990, **44**, 550–561.
- R. Lu, W. W. Li, A. Katzir, Y. Raichlin, B. Mizaikoff and H. Q. Yu, *Analyst*, 2016, **141**, 6061–6067.
- G. Das, F. Mecarini, F. Gentile, F. De Angelis, M. Kumar HG, P. Candeloro, C. Liberale, G. Cuda and E. Di Fabrizio, *Biosens. Bioelectron.*, 2009, **24**, 1693–1699.
- A. I. López-Lorente, B. M. Simonet, M. Valcárcel, S. Eppler, R. Schindl, C. Kranz and B. Mizaikoff, *Talanta*, 2014, **118**, 321–327.
- A. I. López-Lorente, B. M. Simonet, M. Valcárcel and B. Mizaikoff, *Anal. Chim. Acta*, 2013, **788**, 122–128.
- O. Bibikova, J. Haas, A. I. López-Lorente, A. Popov, M. Kinnunen, I. Meglinski and B. Mizaikoff, *Analyst*, 2017, **142**, 951–958.
- H. H. Kyaw, S. H. Al-Harathi, A. Sellai and J. Dutta, *Beilstein J. Nanotechnol.*, 2015, **6**, 2345–2353.
- I. Noda and Y. Ozaki, *Two-dimensional correlation spectroscopy: applications in vibrational and optical spectroscopy*, Wiley, 2004.
- A. I. López-Lorente, J. Izquierdo, C. Kranz and B. Mizaikoff, *Vib. Spectrosc.*, 2017, **91**, 147–156.
- A. I. López-Lorente, R. A. Picca, J. Izquierdo, C. Kranz, B. Mizaikoff, C. Di Franco, S. Cárdenas, N. Cioffi, G. Palazzo and A. Valentini, *Microchim. Acta*, 2018, **185**, 153.
- M. Iosin, F. Toderas, P. L. Baldeck and S. Astilean, *J. Mol. Struct.*, 2009, **924–926**, 196–200.
- L. J. Xu, C. Zong, X. S. Zheng, P. Hu, J. M. Feng and B. Ren, *Anal. Chem.*, 2014, **86**, 2238–2245.
- T. Miura, H. Takeuchi and I. Harada, *Biochemistry*, 1991, **30**, 6074–6080.
- V. J. C. Lin and J. L. Koenig, *Biopolymers*, 1976, **15**, 203–218.
- P. Sevilla, S. Sánchez-Cortés, J. V. García-Ramos and A. Feis, *J. Phys. Chem. B*, 2014, **118**, 5082–5092.
- G. Das, F. Mecarini, F. De Angelis, M. Prasciolu, C. Liberale, M. Patrini and E. Di Fabrizio, *Microelectron. Eng.*, 2008, **85**, 1282–1285.
- N. C. Maiti, M. M. Apetri, M. G. Zagorski, P. R. Carey and V. E. Anderson, *J. Am. Chem. Soc.*, 2004, **126**, 2399–2408.
- S. U. Sane, S. M. Cramer and T. M. Przybycien, *Anal. Biochem.*, 1999, **269**, 255.
- C. J. Suess, J. D. Hirst and N. A. Besley, *J. Comput. Chem.*, 2017, **38**, 1495–1502.
- http://www.horiba.com/fileadmin/uploads/Scientific/Documents/Raman/HORIBA_webinar_proteins.pdf.
- A. Giugliarelli, L. Urbanelli, M. Ricci, M. Paolantoni, C. Emiliani, R. Saccardi, B. Mazzanti, L. Lombardini, A. Morresi and P. Sassi, *J. Phys. Chem. A*, 2016, **120**, 5065–5070.
- T. Arakawa, Y. Kita and S. N. Timasheff, *Biophys. Chem.*, 2007, **131**, 62–70.
- A. Tjernberg, N. Markova, W. J. Griffiths and D. Hallén, *J. Biomol. Screening*, 2006, **11**, 131–137.